Measured Characteristics of the MIMO Wireless Channel

Jon W. Wallace and Michael A. Jensen
Department of Electrical and Computer Engineering
Brigham Young University, Provo, UT 84602-4099

Abstract—**This paper presents results from an experimental platform designed to measure the transfer matrix for indoor and outdoor multiple-input multiple-output (MIMO) channels with up to 16 transmit and receive antenna elements. Key aspects of the hardware system and data post-processing techniques are provided. A variety of measurements have been taken with the platform at 2.45 GHz in a typical indoor environment. The collected data has been processed to highlight a variety of channel features, including the statistical distributions of the channel matrix elements and the inherent capacity of the wireless MIMO channel for different numbers of antenna elements, polarizations, and element directivities.**

I. Introduction

The increasing demand for capacity in wireless systems has motivated considerable research aimed at achieving higher throughput on a given bandwidth. One important finding of this activity is the recent demonstration that for an environment sufficiently rich in multipath components, the wireless channel capacity can be increased using multiple antennas on both transmit and receive sides of the link [1], [2]. Algorithms that achieve this increased capacity actually *exploit* the multipath structure by cleverly coding the data in both time and space. In order to assess the performance of systems that implement these algorithms, we must better understand the complex *spatial* behavior of wireless multiple-input multiple-output (MIMO) channels [3]–[5].

This paper reports the development of and results from an experimental platform designed to probe the transfer matrix for indoor and outdoor MIMO channels. This system has the ability to simultaneously measure up to 16 transmit and receive branches. The key aspects of the hardware system are presented, including a discussion of measurement issues and data processing methodologies. Representative data obtained with the instrument in several indoor environments are also provided, with emphasis placed on key parameters such as channel stationarity, transfer matrix element statistics, spatial correlation, and capacity for a variety of array characteristics.

II. Measurement System

The goal of this effort is to directly measure the wireless MIMO channel transfer matrix $\mathbf{H}$, where the element $H_{mn}(\omega)$ represents the frequency dependent transfer function between the n^{th} transmitter and m^{th} receiver antennas. The experimental platform, depicted in Figure 1, uses a custom MIMO communications system operating between 0.8 and 6 GHz. The transmitter uses a digital pattern generator (DPG) to create N unique binary (± 1) codes. These codes are fed into a custom RF chassis where they are mixed with a local oscillator (LO) to produce N distinct co-channel binary phase shift keyed (BPSK) signals. The resulting signals are amplified to 0.5 W and fed into one of the N transmit antennas.

The receiver uses a custom RF chassis to amplify and down-convert the signals from each of the M antennas. The resulting M intermediate frequency (IF) signals are low-pass filtered, amplified, and sampled using a 16-channel 1.25 Msample/s A/D card for storage on the PC. Two different antenna arrays have been constructed for the experiments. The first design is a 4-element dual-polarization patch array with half-wavelength element spacing. The second consists of a square metal plate with a two-dimensional grid of 33×33 holes spaced at roughly 1.5 cm intervals. Monopole antennas are placed in the holes to achieve a wide variety of array geometries.

III. Data Processing

The raw data collected using the measurement platform is processed to obtain estimates of the time-variant channel matrix. The technique consists of 3 basic steps: (1) code synchronization, (2) carrier recovery, and (3) channel estimation.

A. Code Synchronization

The first step in the data post-processing is to determine the alignment of the modulating codes. As shown in Figure 2, the method begins by correlating the signal from one of the M receive antennas with a baseband representation of one of the transmit codes. A Fast Fourier Transform (FFT) of this result produces a peak at the IF when the known code and the code in the receive signal are aligned. The algorithm expedites the process by using shortened correlating codes and coarse steps at the beginning of the search process, and adaptively reducing the step size and switching to full-length codes as the search converges. Additionally, if the signal carrying the specified code is weak, the maximum correlation may not occur at code alignment. To overcome this, our procedure searches over every combination of receive channel and code to ensure accurate code synchronization.

B. Carrier Recovery

The FFT peak obtained during code synchronization provides an estimate of the IF. This result is refined using a subplex optimization loop that maximizes the magnitude of the Discrete Time Fourier Transform (DTFT) of the despread signal (known aligned code multiplied by the receive signal). Following frequency estimation, the phase variation is recovered by moving a window along the despread signal and correlating this waveform against a complex sinusoid at the IF. The phase of this result represents the phase at the center of the recovery window. An averaging window is then used to smooth this phase estimate.

This work was supported by the National Science Foundation under Wireless Initiative Grant CCR 99-79452 and Information Technology Research Grant CCR-0081476.

0-7803-7005-8/01/$10.00 © 2001 IEEE

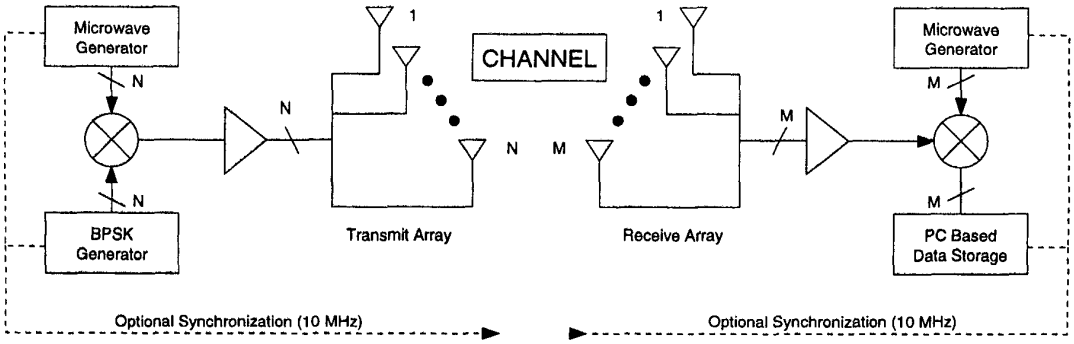

Fig. 1. High level system diagram of the narrowband wireless MIMO measurement system

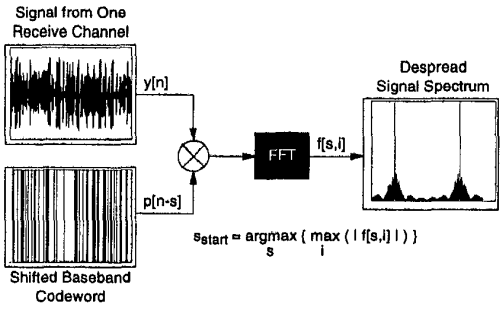

Fig. 2. Basic method for performing code synchronization when the exact carrier frequency is unknown.

TABLE I

MEASUREMENT SYSTEM LOCATIONS WITHIN THE ENGINEERING BUILDING ALONG WITH ANTENNA CONFIGURATIONS.

Name	Xmit Loc	Recv Loc	Ant	Records
4×4(a)	RM484	5 Rooms	4SP	233
4×4(b)	Hall	RM400	2DP	165
10×10(a)	Hall	RM400	10SP	474
10×10(b)	RM484	RM400	10SP	274
10×10(c)	RM484	RM400	10SP	120

C. Channel Estimation

The IF signal on the m^{th} receive channel is composed of N BPSK codes, with each code represented by an amplitude A_{mn} and phase ϕ_{mn}. If $p_n[k]$ represents the k^{th} sample of the n^{th} code, the discrete received signal is given as

$$y_m[k] = \sum_{n=1}^{N} A_{mn}\, p_n[k]\, \cos(\Omega_1 k + \phi_k + \phi_{mn}) + \eta[k] \quad (1)$$

where Ω_1 is the discrete carrier frequency, ϕ_k is the randomly varying carrier phase, and $\eta[k]$ represents the discrete noise sample that is assumed to be spectrally white with a zero-mean Gaussian amplitude distribution.

To construct channel matrices, we must infer the channel parameters A_{mn} and ϕ_{mn} from the received sequence $y_m[k]$. To obtain a maximum likelihood estimation of these values, we multiply $y_m[k]$ by the i^{th} code and the complex signal $c[k] = e^{-j(\Omega_1 k + \phi_k)}$ and subsequently average over $K = (k_2 - k_1 + 1)$ samples to produce

$$R_{mi} = \frac{1}{2K} \sum_{k=k_1}^{k_2} \sum_{n=0}^{N-1} \left[\widetilde{A}_{mn} + \widetilde{A}^{*}_{mn} e^{-j2(\Omega_1 k + \phi_k)} \right] p_{ni}[k] \quad (2)$$

where $p_{ni}[k] = p_n[k] p_i[k]$ and $\widetilde{A}_{mn} = A_{mn} e^{j\phi_{mn}}$. This equation represents a linear system that can be solved for the complex transfer coefficients. The channel matrix elements are then given by $H_{mn} = \widetilde{A}_{mn}$.

IV. Channel Matrix Characteristics

The measurement system was deployed on the fourth-floor of the five-story engineering building on the Brigham Young University campus. This building, constructed with cinder-block partition walls and steel-reinforced concrete structural walls contains classrooms, laboratories, and several small offices. Data were collected at a center frequency of 2.45 GHz using 1000-bit binary codes at a chip rate of 12.5 kbps, yielding a nominal bandwidth of 25 kHz. This chip rate results in channel matrix estimates obtained every 80 ms.

Table I lists the five different locations for the transmit and receive subsystems used in this study. Rooms 400 and 484 are central labs in the building separated by a hallway (designated as "Hall"). "5 rooms" in the table indicates that the receiver was placed at several locations in five different rooms. The specific linear antenna arrays employed were 4 element single polarization patches with $\lambda/2$ spacing (4SP), 2 element dual polarization (V/H) patches with $\lambda/2$ spacing (2DP), and 10 element monopole antennas with $\lambda/4$ spacing (10SP). Data records were each 10-s long.

Since the actual received power varies as a function of the transmit and receive locations, some type of channel normalization is required to facilitate comparison of the results. One reasonable normalization is to scale the channel matrices such that on average, the power transfer between a single transmit and single receive antenna is unity. If $\hat{\mathbf{H}}^{(k)}$ and $\mathbf{H}^{(k)}$ represent the observed and normalized matrices, respectively, at

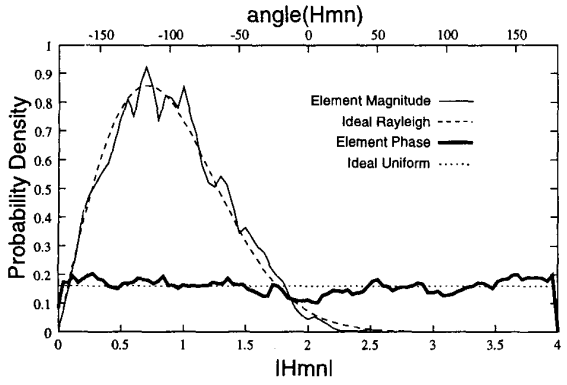

Fig. 3. Empirical PDFs for the magnitude and phase of the 4×4 **H** matrix elements compared with Rayleigh and uniform PDFs, respectively.

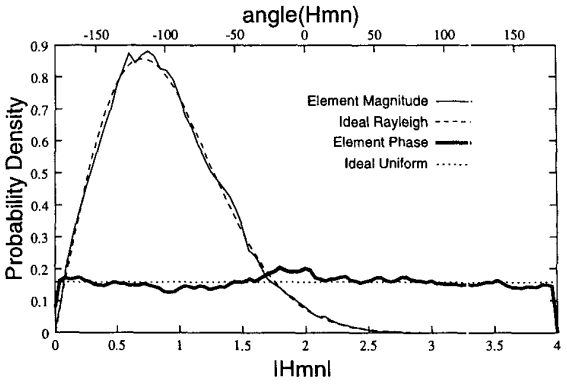

Fig. 4. Empirical PDFs for the magnitude and phase of the 10×10 **H** matrix elements compared with Rayleigh and uniform PDFs, respectively.

time sample k such that $\mathbf{H}^{(k)} = A\hat{\mathbf{H}}^{(k)}$, this constraint yields the normalization constant

$$A = \left(\frac{1}{KMN} \sum_{k=1}^{K} \sum_{m=1}^{M} \sum_{n=1}^{N} |\hat{H}_{mn}^{(k)}|^2 \right)^{-\frac{1}{2}}. \quad (3)$$

If the K matrix samples include the entire data set under consideration, this scaling includes variations due to path loss. If $K = 1$ is used, each individual matrix will produce the same signal-to-noise ratio (SNR). This is useful when assessing the impact of antenna parameters on capacity. Unless specifically stated, data is therefore normalized using $K = 1$.

A. Channel Matrix Element Statistics

We begin this study by presenting the marginal probability density functions (PDF) for the magnitude and phase of the elements of **H**. These empirical PDFs are computed using

$$\left\{ \begin{array}{c} p_{\text{mag}}[x] \\ p_{\text{pha}}[x] \end{array} \right\} = \frac{1}{KMN\Delta x} \underset{K,M,N}{\text{HIST}} \left(\begin{array}{c} |H_{mn}^{(k)}| \\ \angle H_{mn}^{(k)} \end{array}, \Delta x \right) \quad (4)$$

where $\text{HIST}(f, \Delta x)$ represents a histogram of the function f with bins of size Δx and K is the number of **H** matrix samples. In this case histograms are computed by treating each combination of matrix sample, transmit antenna, and receive antenna as an observation.

Figures 3 and 4 show the empirical PDFs for sets 4×4(a) and 10×10(a) respectively. These results are compared with the Rayleigh distribution (magnitude) with parameter $\sigma^2 = 0.5$ and the uniform distribution (phase) on $[-\pi, \pi]$. The agreement between the analytical and empirical PDFs is excellent. The improved fit for 10×10 data arises from more records and antennas available for averaging.

B. Channel Temporal Correlation

The indoor channel is subject to temporal drift due to motion of people, doors, etc. To explore this variation, the temporal autocorrelation function was computed according to

$$X_\ell = \langle H_{mn}[k] H_{mn}^*[k+\ell] \rangle \quad (5)$$

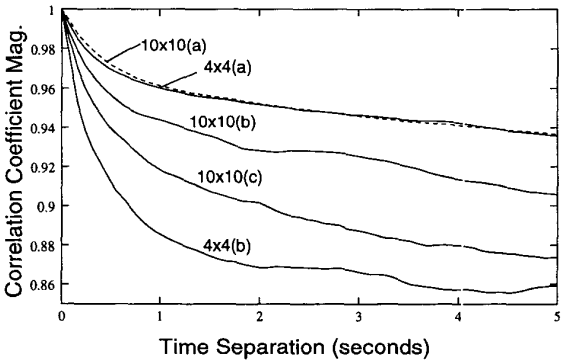

Fig. 5. Temporal correlation coefficient over a 5 second interval for all data sets.

where k is a time sample, ℓ is a sample shift, and $< \cdot >$ represents an average over all combinations of transmit antenna, receive antenna, and starting time sample. The temporal correlation coefficient is then given by $\rho_\ell = X_\ell / X_0$.

Figure 5 plots the magnitude of ρ_ℓ over a period of 5 seconds for each of the data sets considered. We observe that for all measurements, the correlation remains relatively high. This is significant, as it provides insight into the required frequency of training events for MIMO algorithms that use channel state information. We also note that the temporal correlation seems to exhibit an exponential decay to a "resting" value, suggesting that the mean of the channel elements remains relatively constant over the 5-s interval due to the "temporary" nature of the channel disturbances.

C. Channel Spatial Correlation

The channel spatial correlation is an important physical mechanism since lower signal correlation between adjacent antennas tends to produce higher average channel capacity. To examine the channel spatial behavior, we assume a correlation function that is separable in transmit and receive, or

$$R(m,n;i,j) = \text{E}[H_{mn} H_{ij}^*] = R_R(m,i) R_T(n,j) \quad (6)$$

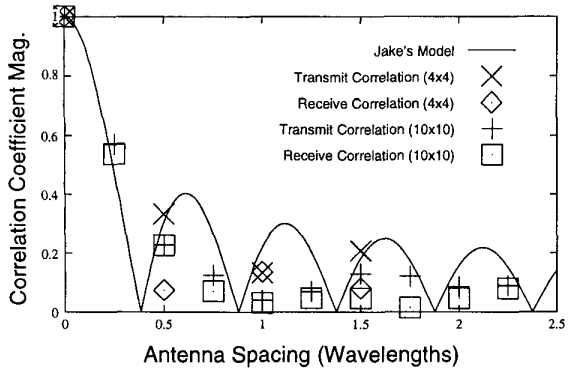

Fig. 6. Magnitude of the shift-invariant spatial correlation coefficients at transmit and receive compared with Jakes' model.

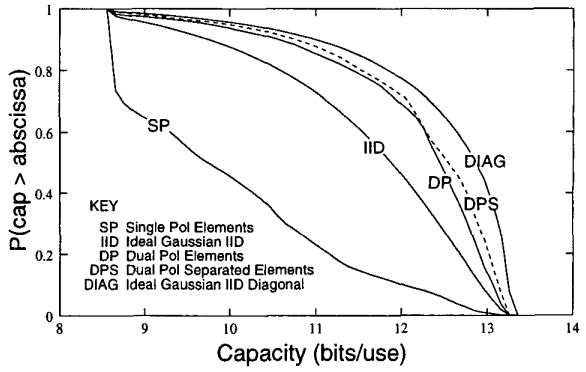

Fig. 7. CCDFs for 2×2 channels employing different types of polarization/spatial separation.

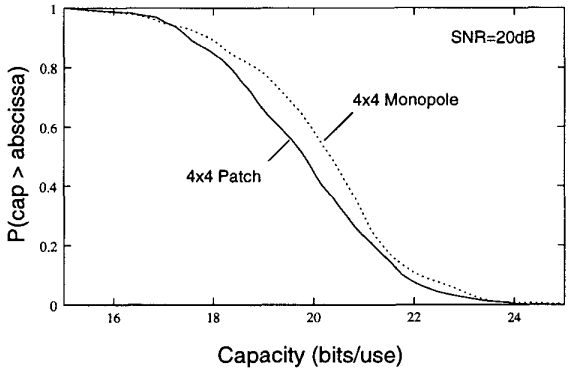

Fig. 8. Capacity CCDFs for 4×4 arrays using omnidirectional monopoles and more directional patch elements.

where $R_R()$ and $R_T()$ represent transmit and receive correlation functions respectively. Figure 6 shows the shift-invariant spatial transmit and receive correlation coefficient compared with Jakes' model [6] where $R_R(i,j) = R_T(i,j) = J_0(2\pi|i-j|\Delta z_\lambda)$ and Δz_λ is the antenna separation in wavelengths. Data sets 4×4(a) and 10×10(a) were used for this example. For this shift-invariant case, we treat all pairs of antennas with the same spacing as independent observations. For small separation, the agreement between the experimental correlation and Jakes' model is very good. The disparity at higher separations is likely due to non-uniform angle of arrival of multipath components as well as a reduced amount of available data for computing the correlation statistics.

V. Channel Capacity

Channel capacity is a key parameter of interest in MIMO architectures. In this study, capacities are computed from the measured **H** matrices according to the water filling solution with an assumed single-input single-output (SISO) SNR of 20dB (see [7]).

A. Polarization Dependence

Using the dual-polarized linear patch array, it is possible to compare the complimentary cumulative distribution functions (CCDFs) of capacity for three different 2×2 channels: (1) 2 elements with same polarization (V or H) but separated by $\lambda/2$, (2) 2 elements which have orthogonal polarization and are colocated, and (3) 2 elements which have both orthogonal polarization and are separated by $\lambda/2$. Figure 7 shows the results of this study. Two single polarization elements (SP) is the inferior case, due to substantial correlation between the elements. The next line on the graph (IID) is the capacity for a 2×2 channel matrix with independent identically distributed (iid) complex Gaussian elements with unit variance, the capacity being computed using Monte Carlo over 10^6 channel realizations. The capacities for the dual polarized elements (DP) and dual polarized elements with separation (DPS) are virtually identical, outperforming the IID case due to the nearly orthogonal channels created (ie nearly diagonal **H** matrix). The final line (DIAG) shows the performance when **H** has iid complex Gaussian elements on the diagonal but is identically zero everywhere else (computed in a manner similar to IID). As expected, this case outperforms our dual-polarization elements which exhibit weak correlation.

B. Directivity Dependence

The monopole antennas employed radiate uniformly in the plane perpendicular to the antennas. The patch antennas, on the other hand, only radiate into a half space. These two types of antennas allow examination of the effect of antenna directivity on channel capacity. Figure 8 plots the capacity of the 4×4 channel for four patch antennas (transmit and receive) from set 4×4(a) and for four monopole antennas using subsets of set 10×10(a). These results indicate that because the omnidirectional antennas intercept all multipath components, they offer improved capacity when compared to the more directive patch antennas.

C. Dependence on Number of Antennas

Naturally, it is not anticipated that the capacity will continue to grow indefinitely as more antenna elements are added. To explore this behavior, we examine the dependence of capacity on the number of antennas for 2, 4, and 10 monopole trans-

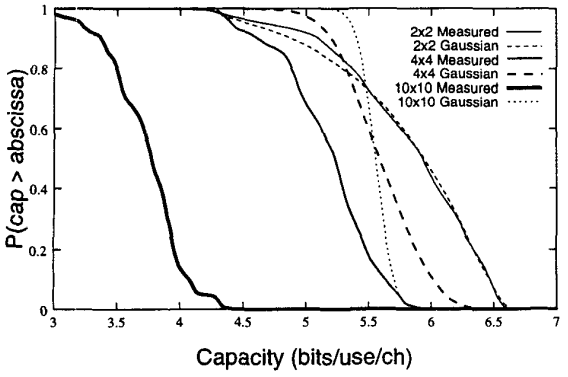

Fig. 9. Capacity CCDFs per number of antennas for transmit/receive arrays of increasing number of elements. The array length is 2.25 λ for all cases.

mit and receive antennas. To make a fair comparison, each array in the study possesses the same total length (2.25λ, using the data from set 10×10(a)). Figure 9 shows the capacity CCDFs per number of transmit and receive antennas. Also, Monte Carlo simulations were performed to obtain capacity CCDFs for channel matrices having iid complex Gaussian elements with unit variance. These results indicate an excellent agreement between the measured 2×2 and ideal 2×2 (independent Gaussian) channel due to the very wide antenna separation (2.25λ). However, as we pack more antennas into our array, the capacity per antenna drops due to higher correlation between adjacent elements.

D. Path Loss Dependence

Path loss is an important parameter to include when studying the capacity of MIMO systems. To highlight the importance of this parameter, a study was performed with several transmit and receive scenarios (using a linear monopole array) as depicted in Figure 10. Each arrow in the figure represents a single scenario with the arrow pointing from transmit location to receive location. The top number in the box on each arrow gives the channel capacity using the standard single **H** matrix normalization ($K = 1$ in Eq. (3)) for 20dB SNR. The second number (in italics) gives the capacity when the normalization is applied over *all* **H** matrices in the study for an average SISO SNR of 20dB. This second value includes the capacity degradation due to path loss. The large variation observed in these numbers demonstrates the importance of including both path loss and multipath richness when comparing the performance of different channels.

VI. Conclusion

Wireless communication systems employing multiple transmit and receive antennas have potentially greater capacity than their single antenna counterparts on the same bandwidth. Understanding the gains that are possible with such systems requires detailed knowledge of the MIMO channel transfer matrix. This paper has presented a system capable of measuring wireless MIMO channel response over the 0.8 to 6 GHz frequency range with up to 16 transmitters and receivers. Details of the required hardware and data processing were outlined along with representative data. The measured data were presented so as to allow assessment of the channel statistical behavior including transfer matrix PDFs and temporal and spatial correlation. Additionally, the impact of polarization, directivity, and number of array elements on channel capacity has been demonstrated. Finally, the importance of including both path loss and multipath richness when comparing capacity of different wireless channels has been illustrated. These results should provide invaluable insight into the behavior of MIMO wireless channels.

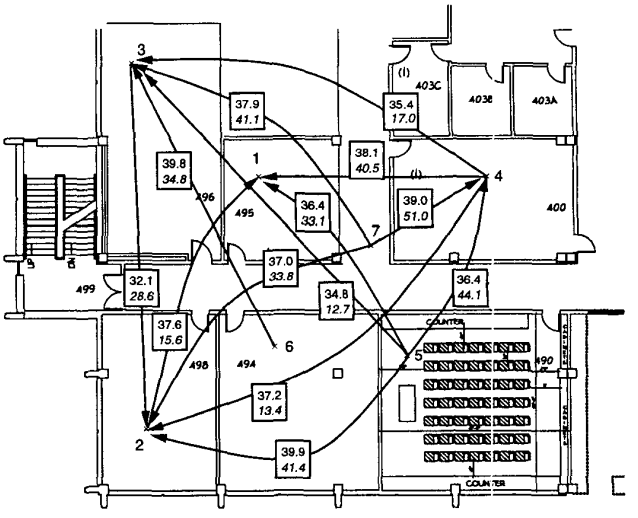

Fig. 10. Study showing the tradeoff between multipath and path-loss with regard to channel capacity. Arrows are drawn from transmit to receive. The top number and bottom number in each box give capacity without and with path loss, respectively.

References

[1] G. J. Foschini and M. J. Gans, "On limits of wireless communications in a fading environment when using multiple antennas", *Wireless Personal Communications*, vol. 6, no. 3, pp. 311–335, March 1998.

[2] G. Golden, C Foschini, R Valenzuela, and P. Wolniansky, "Detection algorithm and initial laboratory results using V -BLAST space-time communication architecture", *Electronic Letters*, vol. 35, no. 1, pp. 14–15, Jan. 1999.

[3] Q. Spencer, B. Jeffs, M. Jensen, and A. Swindlehurst. "Modeling the statistical time and angle of arrival characteristics of an indoor multipath channel", *IEEE J. Selected Areas Commun.*, vol. 18, no. 3, pp. 347–360, Mar. 2000.

[4] C. C. Martin, J. H. Winters, and N. R. Sollenberger, "Multiple-input multiple-output (MIMO) radio channel measurements", in *IEEE Vehicular Technology Conference (Fall VTC 2000)*, Boston, MA, Sep 2000, vol. 2, pp. 774–779.

[5] J. P. Kermoal, L. Schumacher, P. E. Mogensen, and K. I. Pedersen, "Experimental investigation of correlation properties of MIMO radio channels for indoor picocell scenarios", in *IEEE Vehicular Technology Conference (Fall VTC 2000)*, Boston, MA, Sep 2000, vol. 1, pp. 14–21.

[6] W. C. Jakes, *Microwave Mobile Communications*, IEEE Press, 1993.

[7] Gregory G. Rayleigh and John. M. Cioffi, "Spatio-temporal coding for wireless communication", *IEEE Transactions on Communications*, vol. 46, no. 3, pp. 357–366, March 1998.